SELF-CALIBRATION AND EVALUATION OF THE TRIMBLE GX TERRESTRIAL LASER SCANNER

J.C.K. Chow*, W.F. Teskey, and D.D. Lichti

Department of Geomatics Engineering, University of Calgary, 2500 University Dr NW, Calgary, Alberta, T2N1N4 Canada - (jckchow, wteskey, ddlichti)@ucalgary.ca

Commission I, WG I/3

KEY WORDS: Terrestrial, Laser scanning, LIDAR, Calibration, Modelling, Precision, Point Cloud, Analysis

ABSTRACT:

There are numerous imaging modalities for reconstructing 3D object space on the market. Among all the varieties, which include 3D TOF range cameras, structured light systems, and traditional photogrammetric systems, terrestrial laser scanners have gained the most attention and demand from the surveying and engineering discipline. This is probably because of the large field of view and rapid dense data acquisition offered by most modern terrestrial laser scanners. As terrestrial laser scanning is gaining popularity, it is faced with new challenging tasks that demand higher accuracy such as deformation monitoring and other precise engineering applications. To ensure the highest quality point cloud is captured, quality assurance techniques that can be self-deployed before every accuracy demanding application are necessary. The laboratory calibration offered by the manufacturer requires the scanner to be shipped away for weeks, which is too time consuming and expensive to be done frequently. The preferred approach is through a user self-calibration routine. This paper presents the results from two point-based self-calibration campaigns of the Trimble GX, which is Trimble's latest pulse-based hybrid type terrestrial laser scanner on the market.

1. INTRODUCTION

Over the years, terrestrial laser scanning (TLS) has already established its popularity in the surveying, engineering, and mapping industry because of its capability of capturing high density accurate 3D information of the object space. Many terrestrial laser scanners currently on the market can acquire 3D coordinates, object reflectivity, and 8-bits colour information from 3 bands for every object point measured via the attached camera. This essentially produces realistic 3D images of the object space with true scale from a single exposure station. Over the years, TLS systems have became more user-friendly, portable, and accurate that they are being utilized by more users who are non-experts with TLS systems. The recent technological advancements in TLS have opened its commercial markets to even more areas of application that demands accurate 3D imaging, such as deformation monitoring, machine alignment, and human body measurements.

Among all the various methodologies for collecting high quality dense 3D information in a large field of view, TLS instruments are well known by many experts to be one of the best imaging modality that presently exists. Panoramic pulse-based scanners like the Leica Scanstation C10 can observe objects up to hundreds of metres away from the scanner in a 360^o horizontal field of view and 270^o vertical field of view from a single scan. In contrast, the 3D range cameras currently on the market can only capture objects up to a few metres within usually a 40^o by 40^o window. Phase-based laser scanners like the Faro Photon 120/20 can measure in ultra-high speeds up to 976,000 points per seconds allowing 3D information of a panoramic scene to be captured in merely a few seconds. Other terrestrial laser scanners like the Riegl VZ400 can easily be integrated with GPS and INS to make mobile 3D mapping of a large area (e.g. a city) very efficient. The accuracy of these pulse-based and phase-based systems is influenced by the sensor calibration. Unlike bundle adjustment with self-calibration for digital cameras in photogrammetry, self-calibration of TLS systems have not been standardized and is still under research.

Many researchers around the world have independently identified systematic errors in modern TLS instruments that can be modelled mathematically to improve both the precision and accuracy of the acquired 3D point cloud (Bae and Lichti, 2007; Schneider and Schwalbe, 2008; and Molnár et al., 2009). This can be done relatively easily and inexpensively through what is generally called TLS self-calibration. The benefit of this approach over the manufacturer's laboratory calibration is that the scanner does not need to be dissembled, no expensive specialized tools are necessary, and the self-calibration can be performed as frequent as the user desires without the need to ship the laser scanner away for weeks. TLS self-calibration can be broadly classified into point-based (i.e. signalized targets are observed) or feature-based (i.e. planes are observed). Regardless of the source of the observations, a large redundant set of observations needs to be captured with the TLS from multiple positions and different orientations. In this project, the point-based approach described in Lichti (2007) was used to identify and model systematic errors in the GX. It has been reported independently before by Hanke et al. (2006) that systematic errors exist in the GX. In this paper, the GX was calibrated in both a small room and a large room with signalized planar targets. The centroid of all targets was measured in every point cloud using a combination of least-squares plane fitting and circle fitting (Chow et al., 2010a). Since exact point-to-point correspondence exists, the targets from different scans were related mathematically by a 3D rigid body transformation. The modelling of systematic errors was performed in a spherical

* Corresponding author.

coordinate system, which is the coordinate system where TLS instruments make their raw observations.

2. MATHEMATICAL MODEL

Modern TLS systems can have very different architectures, however most TLS systems have the three most fundamental axes, which are the trunnion axis, vertical axis, and the collimation axis. Many of the physical systematic errors that were previously discovered in TLS systems are caused by these three axes not intersecting with each other at a unique point in space and not being mutual orthogonal. To mathematically describe the systematic errors in TLS systems, the modelling can be performed in a spherical coordinate system. This approach is adopted here because despite the fact that most TLS systems outputs X, Y, and Z Cartesian coordinates, the scanner's raw measurements are horizontal circle readings, vertical circle readings, and range observations to the object space. To back-calculate the spherical observations from Cartesian coordinates with the additional parameters (APs), the transformation in Equation 1 can be used

$$\begin{aligned} \rho_{ij} &= \sqrt{x_{ij}^2 + y_{ij}^2 + z_{ij}^2} + \Delta\rho \\ \theta_{ij} &= \tan^{-1}\left(\frac{y_{ij}}{x_{ij}}\right) + \Delta\theta \\ \alpha_{ij} &= \tan^{-1}\left(\frac{z_{ij}}{\sqrt{x_{ij}^2 + y_{ij}^2}}\right) + \Delta\alpha \end{aligned} \tag{1}$$

where ρ_{ij}, θ_{ij}, α_{ij} are the range, horizontal circle reading, and vertical circle reading respectively of point i in scanner space j.
x_{ij}, y_{ij}, z_{ij} are the Cartesian coordinates of point i in scanner space j.
$\Delta\rho$, $\Delta\theta$, and $\Delta\alpha$ are the additional systematic correction parameters for range, horizontal direction, and vertical direction, respectively.

In a single scan captured by the TLS instrument, every point is uniquely determined. With zero degrees of freedom, the APs cannot be determined. In order to perform least squares adjustment and solve for the object space coordinate, exterior orientation parameters (EOPs) of each scan, and APs simultaneously, multiple scans of the same targets from different positions and orientations must be captured and related via the 3D rigid body transformation equation outlined in Equation 2.

$$\begin{aligned} \begin{bmatrix} x_{ij} \\ y_{ij} \\ z_{ij} \end{bmatrix} &= M_j \left(\begin{bmatrix} X_i \\ Y_i \\ Z_i \end{bmatrix} - \begin{bmatrix} X_{oj} \\ Y_{oj} \\ Z_{oj} \end{bmatrix} \right) \\ M_j &= R_3(\kappa_j) R_2(\phi_j) R_1(\omega_j) \end{aligned} \tag{2}$$

where X_i, Y_i, and Z_i are the object space coordinates of point i.
x_{ij}, y_{ij}, and z_{ij} are the Cartesian coordinates of point i in scanner space j.
X_{oj}, Y_{oj}, and Z_{oj} is the position of the scanner j in object space.
ω_j, φ_j, and κ_j are the primary, secondary, and tertiary rotation angles that describes the orientation of scanner j in object space.

To help reduce the correlation that can exist between the EOPs and the APs, various observations that describe the scanner's EOPs can be appended to the mathematical model. For instance, if the scanner is levelled during data acquisition the roll and pitch angles of the scanner should be zero and Equation 3 can be used to describe this mathematically.

$$\begin{aligned} \omega_j &= 0 \\ \phi_j &= 0 \end{aligned} \tag{3}$$

where ω_j and φ_j are the roll and pitch angles of scanner j

Other observations regarding the heading and position of the scanner's origin (intersection of the trunnion, vertical, and collimation axes) in 3D space can also be included. If the scanner is set up in a tribrach and scans were captured at the same location then force centring can be adopted. In this case, the position of the two scans should be identical if no systematic errors exist. This can be described by the relative scanner position equations in Equation 4.

$$\begin{aligned} X_{oj} - X_{ok} &= 0 \\ Y_{oj} - Y_{ok} &= 0 \\ Z_{oj} - Z_{ok} &= 0 \end{aligned} \tag{4}$$

where X_{oj}, Y_{oj}, and Z_{oj} is the position of scanner j and X_{ok}, Y_{ok}, and Z_{ok} is the position of scanner k, and $j \neq k$

If the scanner is force centred and rotated about the tribrachs, then the heading of each scan should differ by 120° ideally. Therefore another set of observation equations that describes the relative heading angle can be written as well, as shown in Equation 5.

$$\kappa_j - \kappa_k = 120^\circ \tag{5}$$

where κ_j and κ_k is the heading of scanner j and k, respectively, and $j \neq k$.

3. EXPERIMENTATION

The Trimble GX hybrid scanner to be calibrated has a horizontal field of view of 360° and an asymmetric vertical field of view of -20° and +40°. The single point accuracy is claimed by the manufacturer to be 12mm at 100m. With autofocus enabled, the spot size is typically 0.3mm at 5m distance. It has real-time automatic level compensation with an operating range of ± 14'. In addition, the GX observes intensity and RGB information for each point with a scanning speed of up to 5000 points per seconds.

The GX was calibrated twice over a two day period at the University of Calgary. Both calibrations were conducted indoors under stable temperature, pressure, and humidity conditions. Signalized paper targets with a 7.5cm radius white

circle centred on a black background printed on an 8½ by 11 inches paper using a LaserJet printer were constructed and used for both calibrations.

The first calibration took place in a classroom 14m long, 11m wide, and 3m high. A total of 162 Targets were taped onto all the walls and the floor, and captured by the scanner six times, each scan had either a different position, orientation, or both. The scanner was setup on a tribrach, standard wooden surveying tripod, and heavy duty spider manufactured from structural steel. The scanner was always levelled and the GX's built-in dual-axis compensator was activated. The scan resolution was set to 1mm in both the horizontal and vertical direction at 1m distance, with every point measured with two distance shots. Three scans were captured at one of the positions but each with a heading that differs by 120° while force centred. Three other scans were acquired at different positions in the room in an attempt to optimize the scanning network geometry and maximizing the baseline distance between stations. Figure 1 shows the target distribution in the room and scanner used in data acquisition.

Figure 1: First calibration room and set up

The following day, the GX was calibrated once again using targets of the same design. The calibration took place in a laboratory with the dimensions 5m by 5m by 3m. There are targets on all four walls, as well as on the ceiling. The scanner was set up on the same tribrach, tripod, and spider as before (Figure 2). A total of four scans were captured with three scans sharing the same position but with headings that differ by 120°, and the fourth scan approximately 1.8m away. The chosen scanning spatial point density was also 1mm at 1m distance with two distance measurements to each point. In addition, the scanner was always levelled and dual-axis compensation was enabled.

Figure 2: Second calibration room and set up

4. RESULTS AND ANALYSIS

4.1 Calibration 1

From the first calibration, 21 of the total 162 targets were removed prior to the adjustment either because that target was only observed in one scan or it was measured with an incidence angle larger than 60°. This is critical because it has been reported by Lichti (2007) and Soudarissanane et al. (2009) that for planar targets, the signal-to-noise ratio of the measured target centroid drops significantly when the incidence angle is greater than 60°. This threshold was adopted and proved to be successful at reducing the number of blunders detected by Baarda's data snooping at 99% confidence level from 73 to 36.

The GX scanner appears to be well calibrated, as only a total of four known physical systematic error terms are statistically significant. In this calibration, the scanner and non-Trimble target combination showed signs of rangefinder offset (a_0) and laser axis vertical offset (a_1), which deteriorate the range measurement precision. The horizontal angle measurements appear to exhibit signs of trunnion axis error (b_0) and horizontal encoder circle eccentricity error (b_1). These systematic errors are modelled as shown in Equation 6. The determined systematic error correction parameters and its corresponding standard deviations are presented in Table 1.

$$\Delta\rho = a_0 + a_1 \sin(\alpha)$$
$$\Delta\theta = b_0 \tan(\alpha) + b_1 \cos(\theta) \quad (6)$$

Table 1: Coefficients of the sensor modelling parameters in the first calibration

Coefficient	Value	Std. Dev
a_0 [mm]	3.6	0.2
a_1 [mm]	-1.6	0.6
b_0 [“]	157.0	26.8
b_1 [“]	29.9	3.2

The unmodelled rangefinder offset appeared as a linear trend in the range residuals versus range plot (Figure 3). After modelling, the linear trend is removed (Figure 4) and the mean residual in distance measurements is reduced from -0.2mm to zero. The horizontal encoder circle eccentricity error is visually identifiable in the residuals of the horizontal direction versus horizontal direction plot (Figure 5) and was modelled as a sinusoidal term, which removed the systematic bias in the residual plot (Figure 6). The laser axis vertical offset has a small magnitude and is therefore difficult to perceive in any of the residual plots. Even though the trunnion axis error has a large magnitude this error cannot be visually interpreted in the residual plots, but nonetheless it exists and is statistically significant. The main reason for this is because of the hybrid architecture of the GX. Systematic errors in the vertical direction were not modelled either because it was not statistically significant or was not solvable like the vertical circle index error, because of the small vertical field of view of the GX and the low levelling precision (Lichti, 2010). Table 2 summarizes the statistics of the registration before and after the self-calibration. Note how the number of blunders is reduced besides the improvements in the raw measurement precision, which is computed using variance component estimation.

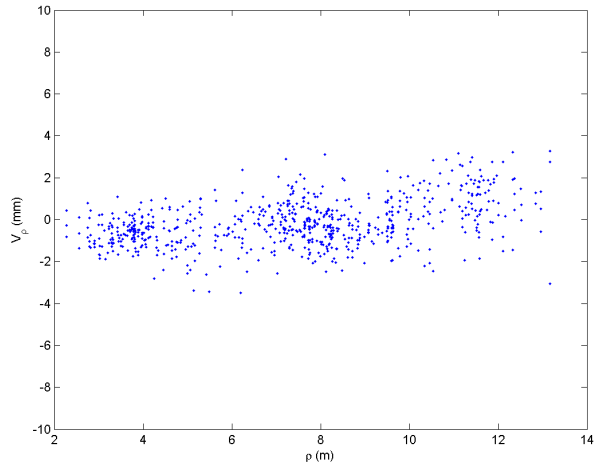

Figure 3: Residuals in range as a function of range *before* the first self-calibration

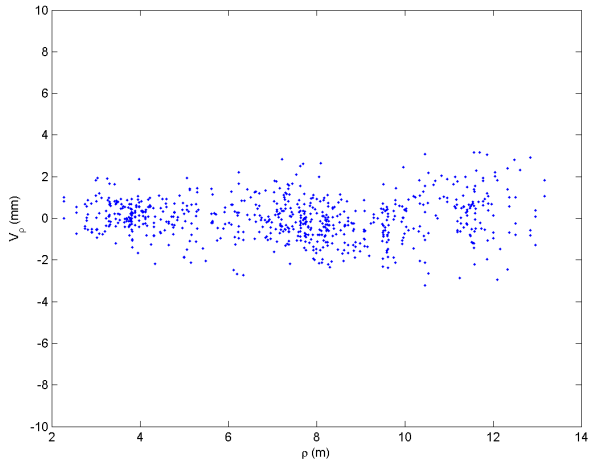

Figure 4: Residuals in range as a function of range *after* the first self-calibration

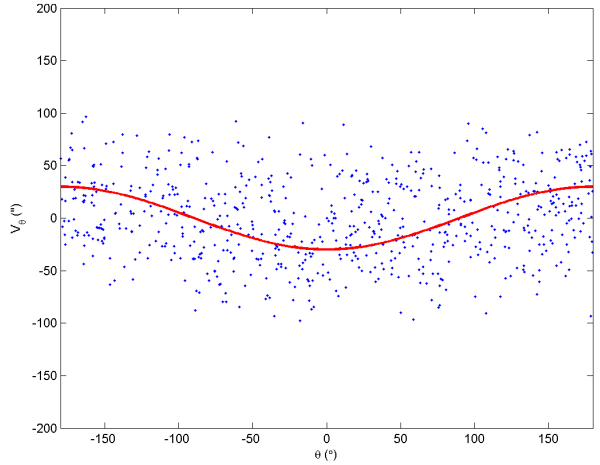

Figure 5: Residuals in the horizontal direction as a function of horizontal direction *before* the first self-calibration

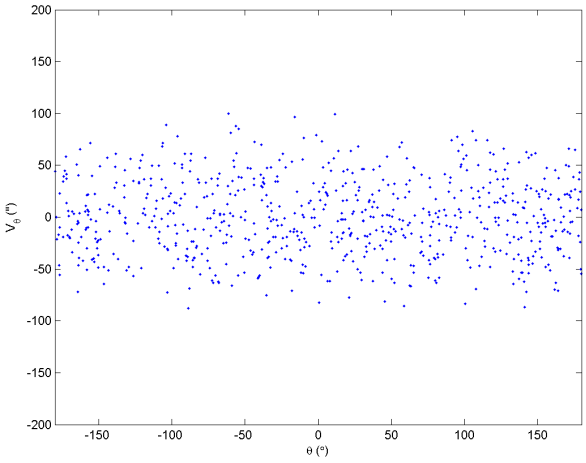

Figure 6: Residuals in the horizontal direction as a function of horizontal direction *after* the first self-calibration

Table 2: Statistics of the first self-calibration before and after sensor error modelling

Parameters	Before Modelling	After Modelling
Number of Targets	141	141
Number of Scans	6	6
Number of Observations	2108	2174
Number of Unknowns	459	463
Redundancy	1653	1715
Average Redundancy	78%	79%
Number of blunders in ρ	22	6
Number of blunders in θ	11	5
Number of blunders in α	3	3
ρ observation precision [mm]	1.3	1.1
θ observation precision ["]	44.6	41.3
α observation precision ["]	23.1	22.6
ρ observation precision improvement [%]	N/A	10
θ observation precision improvement [%]	N/A	7
α observation precision improvement [%]	N/A	2

4.2 Calibration 2

The second self-calibration took place in a smaller room, but with a denser target distribution. As in the first calibration, targets with an incidence angle larger than 60° (19 out of 213) were not included in the adjustment and this reduced the total number of detected blunders using Baarda's data snooping from 11 to 6. A total of seven systematic error terms were found to be statistically significant and were modelled accordingly. The distance measurements exhibit signs of rangefinder offset (a_0) and laser axis vertical offset (a_1), just as in the first self-calibration. The trunnion axis error (b_0) could not be estimated, due to high correlation between b_0 and the scanner's heading (κ). The horizontal direction is modelled by the horizontal encoder circle eccentricity term (b_1), in addition to two more sinusoidal terms that describe the non-orthogonality of the horizontal encoder circle and the vertical axis (b_2 and b_3). Figures 7 and 8 shows the residuals in the horizontal direction as a function of the horizontal direction before and after systematic correction, respectively. Although the scanner was levelled, because of the same reason as in calibration 1, the vertical circle index error was not statistically significant and

strongly correlated with the height of the scanner. A sinusoidal trend in the vertical direction residuals versus horizontal direction plot that was previously discovered in the Trimble (Mensi) GS200 TLS system (Chow et al., 2010b) was found to be statistically significant in this calibration of the GX. The exact cause is still unknown, but it is probably due to the wobbling of the scanner during the scans. Nonetheless, this empirical systematic effect (c_0 and c_1) is observable in Figure 9 and is modelled as a cosine and sine function with a period of 180°, which improves the measurement precision and removes the systematic trend as shown in Figure 10. Equation 7 describes the mathematical model used for modelling the systematic errors inherent in the GX in the second calibration. The APs that were found to be statistically significant in this self-calibration was different from the first calibration. A more extensive math model was used to describe the systematic error behaviour, and the magnitude of some of the common APs changed. The reason for such instability of the determined systematic errors is unknown and is under investigation. The determined coefficients and standard deviation of the mathematical model used for describing the systematic effects are given in Table 3. Table 4 summarizes the statistics of the 3D rigid body transformation before and after sensor modelling.

$$\begin{aligned} \Delta\rho &= a_0 + a_1 \sin(\alpha) \\ \Delta\theta &= b_1 \cos(\theta) + b_2 \sin(2\theta) + b_3 \cos(2\theta) \\ \Delta\alpha &= c_0 \cos(2\theta) + c_1 \sin(2\theta) \end{aligned} \qquad (7)$$

Table 3: Coefficients of the sensor modelling parameters in the second calibration

Coefficient	Value	Std. Dev
a_0 [mm]	1.4	0.3
a_1 [mm]	-2.9	0.6
b_1 [“]	12.1	3.7
b_2 [“]	-4.8	2.2
b_3 [“]	-4.7	2.2
c_0 [“]	4.6	1.3
c_1 [“]	-3.8	1.3

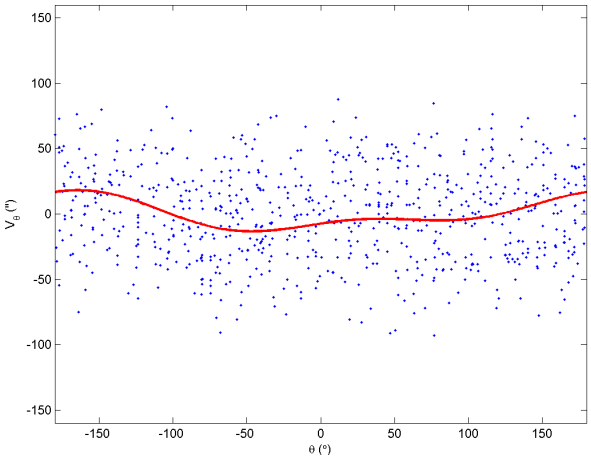

Figure 7: Residuals in the horizontal direction as a function of horizontal direction *before* the second self-calibration

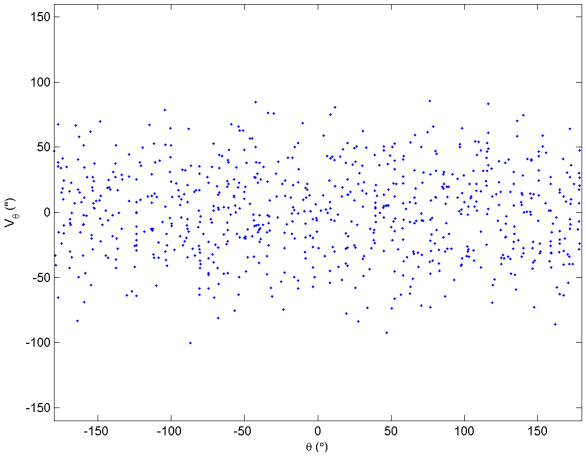

Figure 8: Residuals in the horizontal direction as a function of horizontal direction *after* the second self-calibration

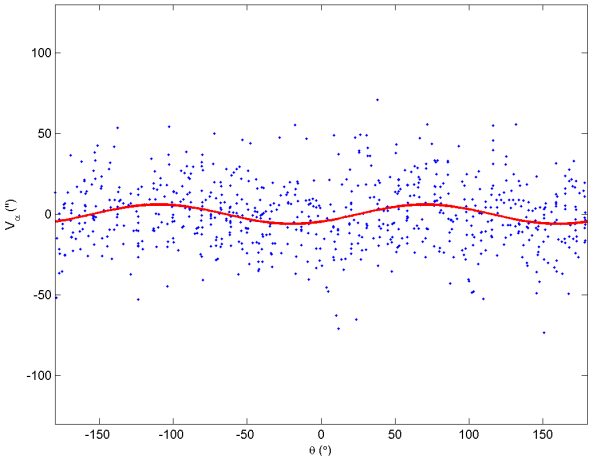

Figure 9: Residuals in the vertical direction as a function of horizontal direction *before* the second self-calibration

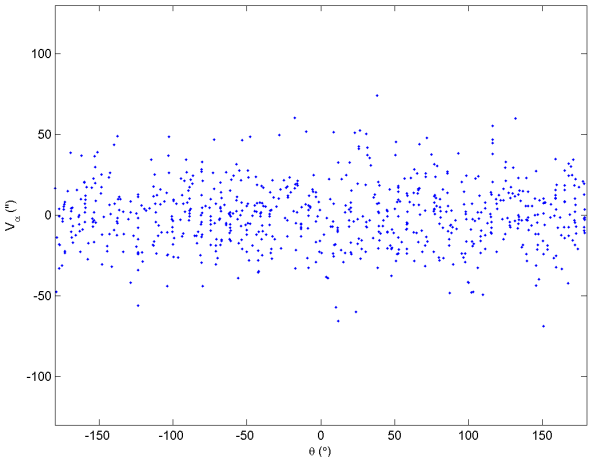

Figure 10: Residuals in the vertical direction as a function of horizontal direction *after* the second self-calibration

Table 4: Statistics of the second self-calibration before and after sensor error modelling

Parameters	Before Modelling	After Modelling
Number of Targets	194	194
Number of Scans	4	4
Number of Observations	2245	2248
Number of Unknowns	606	612
Redundancy	1643	1640
Average Redundancy	73%	73%
Number of blunders in ρ	4	4
Number of blunders in θ	1	0
Number of blunders in α	1	1
ρ observation precision [mm]	1.1	1.1
θ observation precision [“]	41.6	40.5
α observation precision [“]	24.0	23.5
ρ observation precision improvement [%]	N/A	0
θ observation precision improvement [%]	N/A	3
α observation precision improvement [%]	N/A	2

The observations equations that describe the relative position and orientation proposed in this paper appear to have no effect on the self-calibration adjustment. The calibration results presented earlier in this paper included the relative position and heading condition equations, but when compared to the results without these equations the solution was the same. But nonetheless they were presented in this paper to demonstrate the possibility of writing such condition equations and their negligible effects on the correlation, precision, object point coordinates, EOPs, and APs.

5. CONCLUSION

The Trimble GX TLS system was calibrated twice using the point-based self-calibration method. The determined measurement precision of the GX was similar in the two independent calibrations. Slightly different systematic parameters were chosen to model the calibration datasets, but the raw measurement precision computed using variance component estimation were of similar magnitude and improved in both cases. Some of the significant systematic errors could be visually perceived in the residual plots, and through TLS self-calibration it was removed. Other systematic errors like the trunnion axis error may not be observable in the residual plots but can still exist. Also, the relative position and orientation equations suggested in this paper seemed to have negligible effect on the self-calibration of the GX in both cases.

ACKNOWLEDGEMENTS

The authors would like to thank Natural Sciences and Engineering Research Council of Canada (NSERC), Informatics Circle of Research Excellence (iCORE), Cansel, Terramatics Inc., and SARPI Ltd. for funding and supporting this research project.

REFERENCES

Bae, K., & Lichti, D. (2007). On-site self-calibration using planar features for terrestrial laser scanners. *The international Archives of the Photogrammery, Remote Sensing and Spatial Information Sciences 36 (Part 3/W52)* , 14-19.

Chow, J., Ebeling, A., & Teskey, B. (2010a). Low Cost Artificial Planar Target Measurement Techniques for Terrestrial Laser Scanning. *FIG Congress 2010: Facing the Challenges - Building the Capacity.* Sydney, Australia: (On CD-ROM), April 11-16.

Chow, J., Lichti, D., & Teskey, B. (2010b). Self-calibration of the Trimble (Mensi) GS200 Terrestrial Laser Scanner. *ISPRS Commision V Mid-Term Symposium, "Close range Image Measurement Techniques", June 22-24.* Newcastle upon Tyne, United Kingdom. (In Press).

Hanke, K., Grussenmeyer, P., Grimm-Pitzinger, A., & Weinold, T. (2006). First experiencs with the Trimble GX scanner. *In: IAPRS, XXXVI, 5.* Dresden, Germany.

Lichti, D. (2007). Modelling, calibration and analysis of an AM-CW terrestrial laser scanner. *ISPRS Journal of Photogrammetry and Remote Sensing 61 (5)* , 307-324.

Lichti, D. (2010). Terrestrial laser scanner self-calibration: correlation sources and their mitigation. *ISPRS Journal of Photogrammetry and Remote Sensing 65(1)* , 93-102.

Molnár, G., Pfeifer, N., Ressl, C., & Dorninger, P. N. (2009). Range calibration of terresrial laser scanners with piecewise linear functions. *Photogrammetrie, Fernerkundung, Geoinformation 1* , 9-21.

Schneider, D. (2009). Calibration of a Riegl LMS-Z420i based on a multi-station adjustment and a geometric model with additional parameters. *The international Archives of the Photogrammetry, Remote Sensing and Spatial Information Sciences 38 (Part 3/W8)* , 177-182.

Soudarissanane, S., Lindenbergh, R., Menenti, M., & Teunissen, P. (2009). Incidence angle influence on the quality of terrestrial laser scanning points. *In: Proceedings ISPRS Workshop Laserscanning, September 1-2, Volume XXXVIII, Part 3/W8*, (pp. 183-188). Paris, France.